Lifetime of metastable states in a Ginzburg-Landau system: Numerical simulations at large driving forces

A. Umantsev

Department of Physical Chemistry, National University of Science and Technology MISiS, 4 Leninsky Ave, 119049 Moscow, Russia and Department of Chemistry and Physics, Fayetteville State University, Fayetteville, North Carolina 28301, USA

(Received 5 February 2016; published 28 April 2016)

We developed a "brute-force" simulation method and conducted numerical "experiments" on homogeneous nucleation in an isotropic system at large driving forces (not small supersaturations) using the stochastic Ginzburg-Landau approach. Interactions in the system are described by the asymmetric (no external field), athermal (temperature-independent driving force), tangential (simple phase diagram) Hamiltonian, which has two independent "drivers" of the phase transition: supersaturation and thermal noise. We obtained the probability distribution function of the lifetime of the metastable state and analyzed its mean value as a function of the supersaturation, noise strength, and volume. We also proved the nucleation theorem in the mean-field approximation. The results allowed us to find the thermodynamic properties of the barrier state and conclude that at large driving forces the fluctuating volumes are not independent.

DOI: 10.1103/PhysRevE.93.042806

I. INTRODUCTION

The problem of decomposition of a *metastable state* and emergence of a stable one is central not only to physics of materials but also to many branches of science overall. Although the main reason for the decomposition—instability of the state—is the same in all situations, actual realization of it may differ considerably. Actual transformation from the old phase (α) to the new phase (β) may proceed through a process of *nucleation*, that is, overcoming of a barrier state in the form of a *nucleus* or nuclei—small regions of the phase α that acquire properties of the phase β. In many cases, the nucleation occurs due to the presence of foreign objects in the system or specific properties of the walls of a container that encompasses it. This type of nucleation is not a subject of the present publication. We consider only the case of *homogeneous nucleation* when the decomposition is a completely intrinsic phenomenon that comes about as a result of the presence of *thermal fluctuations* in the system. A unique feature of the homogeneous nucleation process is that the thermodynamic work of creation of the nucleus comes directly from the energy of fluctuations while typically the fluctuations have an opposite effect of degrading the energy of the system available for productive work—the free-energy concept.

All theories of nucleation consist of three components in various proportions: thermodynamic properties of the barrier state, account of the fluctuations, and the rate (kinetics) mechanism. Cluster models of nucleation, like classical nucleation theory (CNT) [1–3], consider small aggregates of atoms or molecules as precursors of the new phase, which constantly form and decompose in the old phase due to fluctuations. Many phase transformations in spatially extended systems have been successfully analyzed by continuum theories, like the density functional theory, which is a formulation of statistical physics with the free energy as a functional of the particle number-density distribution [4]. Another continuum theory often used to study nucleation is the diffuse interface theory, which takes into account the nonsharpness of the cluster interface allowing for a size-dependent surface tension [5]. In the *Ginzburg-Landau* (GL) *approach* [6–14] a system is considered as a continuous medium whose state is described by one or more continuous functions of space and time—*order parameter* fields—and properties—by an effective Hamiltonian [6,7]. A great advantage of the GL approach to the nucleation theory is that it self-consistently incorporates all three components of a nucleation theory.

An efficient way to analyze the nucleation problem in the GL framework is to use the concept of *lifetime* [8–14], which is similar to that of the first passage time. According to Penrose and Lebowitz [15], a metastable state is a state in the vicinity of which the representative point of the system spends long time before eventually leaving it with low probability of return. Then the lifetime of a metastable state (the first passage time) can be defined as the time for the representative point to leave the basin of the state. Thermodynamically, the latter means crossing of the barrier by forming a supercritical nucleus. Although the concept of lifetime avoids a multiple nuclei scenario, which is important in experimental situations, it is a potent idea in the theory of nucleation. Two methods are most often employed in order to compute the lifetime in continuous systems: the Ising- type discrete and the analytical continuous methods. In the framework of the first one, the infinite-dimensional continuous system is broken into a large but finite set of cells and the spatially continuous function is replaced by the set of discrete variables. Then the lifetime is calculated for the multivariable finite system. In the second one, the real-valued partition function of the infinite-dimensional continuous system is extended from the domain of parameters where the phase is stable into the domain where the system is metastable or unstable and, therefore, the partition function becomes complex. Then, the imaginary part of the latter is declared to be (proportional to) the lifetime [8,10].

Langer [8] introduced the GL approach to the statistical nucleation theory by describing the phase space of the system with an order parameter taken at a certain number of fixed space points. He obtained an equation for the probability current density in the phase space and found its stationary solution when the system is close to the phase-coexistence line. The lifetime in Langer's theory is estimated as the inverse of the probability current at the saddle point of the Hamiltonian.

Buttiker and Landauer [9] applied Langer's theory to a multisaddle system. Klein *et al.* [10] extended the Langer's theory on the systems close to the spinodal point that is, the point of a barrierless transition. Binder [11] considered the relaxation process in a metastable state using the GL approach and erroneously concluded that "true nucleation is absent in the Ginzburg-Landau model." Patashinskii and Shumilo [12] developed a consistent field theory of decomposition of metastable states in conserved and nonconserved systems and calculated the lifetimes of the states as functions of the "driving force." As a state variable, they used radius of the nucleus, which is a well-defined quantity near the coexistence line but becomes ill defined near the spinodal point. A significant amount of research has been done on the nucleation in one-spatial dimension (1D) systems [9,13,14,16,17]. Umantsev and Olson [11] studied thermodynamic properties of the critical nucleus; Maier and Stein [14] found complicated dependence of the lifetime on the system's size; a group of French researchers [16,17] found that the duration of reactive trajectories between metastable states of equal energy levels follows Gumbel distribution.

Homogeneous nucleation is a strongly nonequilibrium nonlinear stochastic process. Many complex problems where fluctuations are important require numerical calculations as an effective tool of their solution. Monte Carlo (MC) and molecular dynamics (MD) methods were used for direct or "brute-force" simulations of the nucleation process on the intermolecular level. Tomita and Miyashita [18] conducted MC simulations of the nucleation process in a metastable state of a two-dimensional (2D) Ising model and found that the mean lifetime was inversely proportional to the volume of the system for small driving forces but independent of the size for the large driving forces with the driving-force depended crossover. Rahman *et al.* [19] used MD simulations to study crystal nucleation in a Lennard-Jones system and found that the lifetime of the quenched state depends on the interaction potential. Yasuoka and Matsumoto [20] carried out a large-scale MD simulation of the vapor-to-liquid transition with water molecules interacting via either Lennard-Jones or water-water potential. The nucleation rate, which is inversely proportional to the lifetime, was estimated based on the number of clusters exceeding a predefined threshold size and plotted as a function of time. The critical nuclei happened to be in the range of 30–45 water molecules. "Brute-force" simulations are limited to situations in which the activation barrier is not very high. If the activation barrier is too high, then the spontaneous crossing of the barrier becomes very unlikely and cannot be observed in the limited time accessible in simulation. In such cases, one has to resort to indirect and more complicated techniques such as umbrella sampling [21], transition-path sampling [22], or multilevel splitting [17].

Nucleation rate depends strongly on the free-energy landscape of the system. Much effort has been made to verify the Gibbsian concept of the free-energy barrier and develop numerical methods for the free-energy landscape evaluation. Frenkel *et al.* [23] used MD simulation to determine the nucleation barrier in colloidal systems. Recently, Wedekind *et al.* [24] introduced a new method based on the concept of mean first-passage time, which allowed them to evaluate the nucleation barrier in MD simulations of a Lennard-Jones gas.

There are two types of numerical simulation approaches to the homogeneous nucleation, which use the GL method. In the first one [25], one randomly incorporates the critical nuclei into the system using probabilities calculated from CNT and allows the system to evolve from that state onward. In the second one [26,27], one incorporates the thermal noise in the form of a Langevin stochastic force into the time-dependent GL equation, which turns the order-parameter evolution into a stochastic process. Petschek and Metiu [26] used the Cahn-Hilliard-Langevin equation for concentration in a binary alloy, which undergoes spinodal decomposition and calculated the correlation functions and structure factor. Vilas and Mazenko [27] analyzed domain growth kinetics in the GL system and found that the numerical results are consistent with the theoretical ones. Langevin dynamics is known to have strong connections with that of Monte Carlo method of treating stochastic processes. Meakin *et al.* [28] compared the two methods for the spinodal decomposition and found them equivalent.

However, it is important to stress that, despite significant effort of the researchers, the statistical properties and functional dependency of the nucleation rate on the control parameters remain largely unexplored in the 3D field systems. In this publication we use the stochastic GL approach to conduct numerical simulations of the homogeneous nucleation in an isotropic 3D system at large (not small) values of the driving force and calculate the lifetime at various values of the driving force, thermal noise, and system volume. In Sec. II we review basic results of the GL equilibrium theory as applied to the thermodynamic and fluctuation properties related to nucleation. In Sec. III we discuss the stochastic dynamics in the GL framework, construct the direct simulation method, provide the simulation results, and analyze them theoretically. In Sec. IV we discuss the successes and failures of the method and consider real-material systems applications.

II. EQUILIBRIUM SYSTEM

A. Thermodynamic theory and free-energy landscape

In the GL approach, the states of the system are described by different distributions of an *order parameter* (OP) scalar field $\eta(\mathbf{x})$. Interactions in an isotropic system of volume V are described by the GL effective Hamiltonian [6–12]:

$$\mathcal{H}\{\eta\} = \int_V d^3x \left[H(\eta;\mu) + \frac{1}{2}\kappa(\nabla\eta)^2 \right], \tag{1}$$

which consists of the uniform contribution described by the Hamiltonian density $H(\eta;\mu)$ and the spatially inhomogeneous contribution proportional to the stiffness parameter κ. The latter depends on the radius of intermolecular interactions responsible for the α/β phase transitions. μ is the *chemical potential difference* between the α and β phases, which is a quantitative expression of the deviation from the α/β equilibrium (sometimes called the "driving force"). It is a matter of convenience to choose the reference "disordered" state α such that $\{\eta_\alpha = 0, \mu_\alpha = 0, H(\eta_\alpha;\mu_\alpha) = 0\}$.

In addition to the Hamiltonian, the state is characterized by its *volumetric content*, that is, excess order counted from the

disordered state:

$$v\{\eta\} \equiv \int_V d^3x\,\eta(\mathbf{x}). \tag{2}$$

If the fluctuations of the OP are not important (e.g. at low temperatures), then the effective Hamiltonian, Eq. (1), is equal to the *Helmholtz free-energy excess* counted from the free energy of the α state F_α [6]:

$$F\{\eta\} - F_\alpha \equiv \Delta F = \mathcal{H}\{\eta\}. \tag{3}$$

In the functional space of the OP, *equilibrium states* of the system are found among the extremals $\eta_E(\mathbf{x})$ of the functional $\mathcal{H}\{\eta\}$, that is, solutions of the Euler-Lagrange equation (ELE) [7,8,10,12]:

$$\frac{\delta\mathcal{H}}{\delta\eta} \equiv \frac{\partial H}{\partial\eta} - \kappa\nabla^2\eta = 0, \tag{4}$$

which satisfy *boundary conditions* (BC) corresponding to the physical problem under consideration. In this publication, we consider a system with a free boundary where the Newmann-type BC apply:

$$\mathbf{n}\nabla\eta(\mathbf{x}) = 0 \quad \text{on} \quad \tilde{V}. \tag{5}$$

If we apply to Eq. (1) formula $\nabla(\eta\nabla\eta) = \eta\nabla^2\eta + (\nabla\eta)^2$, the Gaussian theorem, ELE, Eq. (4), and BC, Eq. (5), then the free-energy excess, Eq. (3), can be expressed as follows [7]:

$$\Delta F_E = \int_V d^3x\left[H(\eta_E;\,\mu) - \frac{1}{2}\eta_E\frac{\partial H}{\partial\eta}(\eta_E;\,\mu)\right]. \tag{6}$$

Three sets of equilibrium states are of particular importance here: uniform, kink-type, and localized nonuniform. The OP of the former are solutions of the homogeneous equation: $\partial H(\eta_E)/\partial\eta = 0$. A system with a nonconvex Hamiltonian density H(η) has more than one uniform equilibrium state. Stable or metastable uniform states are called *phases*; in the OP space they are separated by unstable uniform equilibrium states called *transition states*. The free-energy excesses and volumetric contents of the uniform states are proportional to the occupied volume V. The OP of a kink-type state is a 1D solution of Eq. (4): $\eta_E(\mathbf{x}) = \eta_I(x)$; it represent an *interface* separating the coexisting phases. Its free-energy excess is proportional to the surface area S separating the phase volumes. A localized nonuniform equilibrium state represents a barrier state between the metastable and stable phases: $\eta_E(\mathbf{x}) = \eta_B(\mathbf{x})$; it is called a *critical nucleus*. The free-energy excess ΔF_B and volumetric content $\mathcal{V}_B$ of the critical nucleus are positive and finite, that is, not proportional to V. Notice that the freeenergy excess of an equilibrium state $\eta_E(\mathbf{x})$ is equal to the work that must be done on the homogeneous state $\eta = \eta_\alpha$ in order to form that state in an open system.

In this publication we consider a typical first-order phase transition between two phases, α and β, e.g., crystallization or polymorphism, caused not by temperature changes but by changes of pressure, concentration, or another thermodynamic quantity. Traditionally, the first-order transitions have been studied in the framework of a symmetric 2-4-Landau Hamiltonian with a linear biasing proportional to the external field, e.g., electric or magnetic. However, in liquid-solid and polymorphic transitions the phase biasing is delivered by the *chemical potential difference,* not the external fields. In this case, an efficient way to study the phenomena of phase coexistence, nucleation, growth, and coarsening in the GL framework is to consider the Hamiltonian density in the form:

$$H(\eta;\mu) = \tfrac{1}{2}W\omega^2(\eta) + \mu\,\nu(\eta); \tag{7a}$$

$$\omega(\eta) = \eta(1-\eta), \quad \nu(\eta) = \eta^2(3-2\eta), \tag{7b}$$

where $W = \text{const}$ is the scale of the energy barrier and $\mu = \text{const}(T)$ is the chemical potential difference [29]. Such Hamiltonian is called *asymmetric*, *athermal*, and *tangential* [7]. It guarantees that the OP values of the disordered α ($\eta_\alpha = 0$) and ordered β ($\eta_\beta = 1$) phases are independent of μ. Notice that for the athermal Hamiltonian the excesses of the free and internal energies are equal. For convenience, we define dimensionless *supersaturation* as follows:

$$\Delta \equiv -\frac{6\mu}{W}. \tag{8}$$

Then $\Delta = 0$ is the α/β-phase equilibrium point; $\Delta = 1$ is the α-phase *spinodal* point; for $0 < \Delta < 1$ the α phase is metastable with $\Delta F_\beta = -VW\Delta/6$; and the transition state between α and β phases has $\{\eta_t = (1-\Delta)/2,\ \Delta F_t = VW(3+\Delta)(1-\Delta)^3/96\}$.

At $\Delta = 0$ there exists an equilibrium interface $\eta_E(\mathbf{x}) = \eta_I(x)$ between the α and β phases and the 1D ELE, Eq. (4), can be written as

$$R_0\frac{d\eta_I}{dx} = \pm\eta_I(1-\eta_I)\,, \tag{9}$$

where $R_0 = (\kappa/W)^{1/2}$ is the *GL radius of interactions*. Equation (9) has a two-branch hyperbolic-tangent solution [7] with the interfacial energy excess

$$\frac{\Delta F_I}{S} \equiv \sigma = \int_{-\infty}^{+\infty}\left(\frac{d\eta_I}{dx}\right)^2 dx = \frac{\sqrt{\kappa W}}{6}. \tag{10}$$

To find the structure and thermodynamic properties of the critical nucleus in the isotropic system described by the Hamiltonian, Eqs. (1) and (7), one has to resolve the 3D spherically symmetric ELE, Eq. (4), with BC, Eq. (5). Solutions of this problem $\eta_E(\mathbf{x}) = \eta_B(r)$ for different values of the supersaturation are obtained in Appendix A and plotted in Fig. 1. In the small supersaturation limit ($\Delta \to 0$) it resembles the 1D kink-type solution where all the changes localized at a well-defined boundary of the critical nucleus. In the large (not small) supersaturation limit ($\Delta \to 1$) it is a bell-type curve localized at the center of the nucleus with the maximum height significantly smaller than $\eta_\beta = 1$ [10]. The radius of the critical nucleus can be estimated as $R_N = 2R_0/\Delta$ in the limit $\Delta \to 0$ and $R_C = R_0/(1-\Delta)^{1/2}$ in the limit $\Delta \to 1$.

In Fig. 2, the free-energy excess ΔF_B and volumetric content $\mathcal{V}_B$ of the critical nuclei are plotted as functions of the supersaturation Δ (see Appendix A). Notice sharp decrease of the excess energy and the slow rise of the excess order with the approach to the spinodal point.

Nucleation theorem is a general relation between the free-energy excess, size of the critical nucleus, and the chemical potential difference in the system [3,30]. Equations (1)–(7) allow one to establish it in the mean-field approximation (see

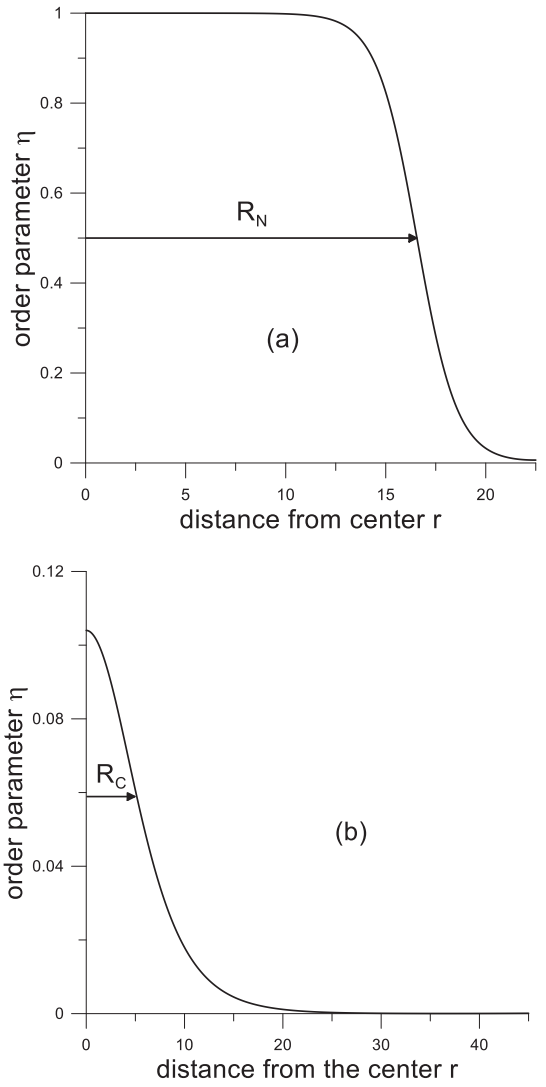

FIG. 1. Numerically calculated radial distributions of the OP field of the critical nuclei $\eta_B(r)$ for (a) small ($\Delta = 0.12$) and (b) large ($\Delta = 0.95$) supersaturations (see Appendix A).

Appendix C):

$$\frac{\partial \Delta F_B}{\partial \mu} \approx v_B. \tag{11}$$

Derivation in Appendix C shows that the nucleation theorem, Eq. (11), is accurate as long as the thickness of the interface region is much smaller than the radius of the critical nucleus: $2R_0 \ll R_N$. Hence, in the mean-field approximation, the nucleation theorem is true only in the limit $\mu \to 0$ ($\Delta \to 0$). In the limit $\Delta \to 1$, due to the diffuseness of the barrier state, Eq. (11) does not hold and the respective relation should be established directly from Eqs. (1)–(8), see Appendix A and Fig. 2.

B. Fluctuation theory

Presence of the thermal noise in the system causes fluctuations of the OP field $\eta(\mathbf{x})$ and changes properties of the system. In the Gibbs canonical ensemble, the statistical

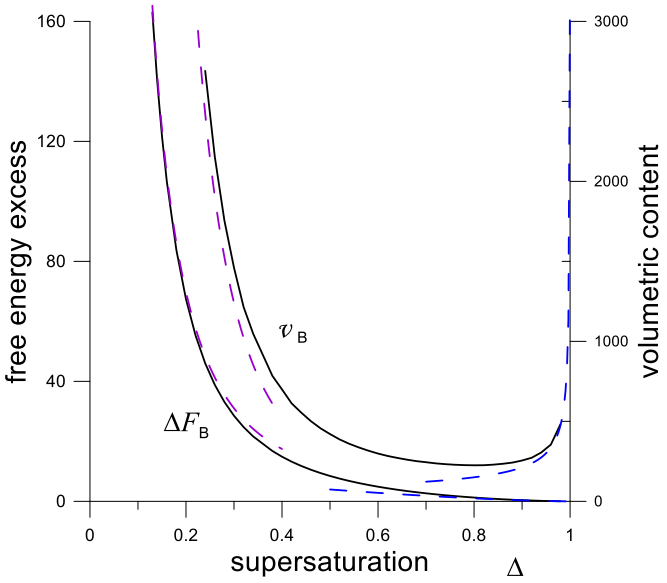

FIG. 2. Free-energy excess ΔF_B and volumetric content v_B of the barrier state as functions of the supersaturation Δ, see Appendix A. Black solid lines correspond to the intermediate supersaturations computed numerically; purple dash, small supersaturation limit, Eqs. (A14) and (A15); blue dash, large supersaturation limit, Eqs. (A21) and (A22).

average of a fluctuating thermodynamic quantity $Q\{\eta\}$ is expressed as $\langle Q\rangle \equiv \frac{1}{Z}\int D\eta Q\{\eta\}e^{-\beta\mathcal{H}\{\eta\}}$, where $\beta = 1/k_BT$, k_B is Boltzmann's constant, T is the temperature of the ensemble, $\mathcal{Z} \equiv \int^D \eta\ e^{-\beta\mathcal{H}\{\eta\}}$ is the fluctuation partition function of the system, and $\int^D \eta \equiv \prod_{\mathbf{x}\in V}\int^D \eta(\mathbf{x})$ denotes the functional integration over all possible configurations of the OP field. The fluctuation Helmholtz free energy F and internal energy E are defined as follows:

$$F\{\eta\} - F_\alpha \equiv \mathcal{F} = -\beta^{-1}\ln Z, \tag{12}$$

$$\langle\mathcal{H}\rangle \equiv \mathcal{E} = \frac{\partial(\beta\mathcal{F})}{\partial\beta}. \tag{13}$$

In Ref. [31] the low-temperature fluctuation-perturbation theory was developed and the fluctuation energies and volumetric content, Eq. (2), together with their variances, were calculated in the second-order expansion in the small noise intensity β^{-1}. The small parameter of expansion was dimensionless strength of noise:

$$\varepsilon \equiv \frac{1}{\beta W R_0^3} = \frac{T}{T_F}; \tag{14a}$$

$$T_F \equiv \frac{\kappa R_0}{k_B}, \tag{14b}$$

where T_F is the GL fluctuation temperature scale. The leading terms of the expansions are the following:

$$\mathcal{E}_0 = \frac{V}{2\beta R_0^3} = \frac{1}{2}\varepsilon W V\ , \tag{15a}$$

$$\mathrm{Var}(\mathcal{H}) = \frac{\mathcal{E}_0}{\beta}, \tag{15b}$$

$$\mathcal{F} = \mathcal{E}_0\left\{\ln\frac{\beta W V[1-\Delta+(6\pi^2)^{2/3}]}{2\pi} - \frac{2}{3} + \frac{2}{U^2}\left(1-\frac{\tan^{-1}U}{U}\right)\right\}, \quad (15c)$$

$$\langle v\rangle = \frac{1}{\pi}\left(\frac{6}{\pi}\right)^{1/3}\frac{3-\Delta}{1-\Delta}\left(1-\frac{\tan^{-1}U}{U}\right)\frac{\mathcal{E}_0}{W}, \quad (15d)$$

$$\mathrm{Var}(v) = \frac{V}{\beta W(1-\Delta)}, \quad (15e)$$

where $U = (6\pi^2)^{1/3}(1-\Delta)^{-1/2}$. Notice that Eqs. (15c) and (15d) represent a "fluctuation theorem"—a relationship among the fluctuation free energy, volumetric content, and the driving force.

III. NUMERICAL SIMULATIONS

A. Stochastic dynamics

In this publication, we analyze fluctuations in the system described by a nonconservative OP filed. The evolution of such a system close to the state of its equilibrium is described by the stochastic time-dependent Ginzburg-Landau equation (STDGLE):

$$\frac{d\eta}{dt} = -\gamma\frac{\delta\mathcal{H}}{\delta\eta} + \xi(\mathbf{x},t). \quad (16)$$

Here t is time, γ is the GL relaxation coefficient, and ξ is the Langevin random force, which mimics the internal noise. If the noise is thermal and "white," then it obeys the following correlation conditions:

$$\langle\xi(\mathbf{x},t)\rangle = 0, \quad (17a)$$

$$\langle\xi(\mathbf{x},t)\xi(\mathbf{x}',t')\rangle = 2\gamma\beta^{-1}\delta(\mathbf{x}-\mathbf{x}')\delta(t-t'), \quad (17b)$$

where the averaging is over the time sequence. As known [6–8], STDGLE, Eqs. (16) and (17), are consistent with the thermal equilibrium in the canonical ensemble.

In the framework of the direct ("brute-force") simulations method, Eqs. (16) and (17) are discretized using the space-time grid with parameters Δx and Δt and solved numerically starting with the initial value of $\eta(\mathbf{x}) = \eta_\alpha = 0$. For convenience the following scaling for the space, time, and energy are used:

$$\frac{x}{R_0}\to x;\ \frac{V}{R_0^3}\to V;\ \frac{t}{\tau}\to t;\ \frac{\mathcal{H}}{WR_0^3}\to\mathcal{H};\tau\equiv\frac{1}{\gamma W}; \quad (18)$$

where τ is the GL time scale. Other details of the "brute-force" method are described in Ref. [31] where its consistency with the fluctuation-perturbation theory, Eq. (15), was verified and the optimal scaled grid parameters were found: $\Delta x = 2$, $\Delta t = 0.5$.

In the next subsection are presented results of numerical simulations for the asymmetric, athermal, and tangential Hamiltonian, Eqs. (1) and (7), with the dimensionless control parameters varied in the following ranges: supersaturation $\Delta = 0.5$–0.95, noise strength $\varepsilon = 9\times10^{-4} - 9\times10^{-2}$, and volume $V = 3.375\times10^6 - 6.4\times10^7$. As the system starts in the homogeneous α state $\eta_\alpha = 0$, there is a relaxation process to reach the metastable state with fluctuations. The nucleation is considered to have taken place if at least one of the points in the system has $\eta(\mathbf{x}_c) \geqslant \eta_\beta = 1$; this point is called the *center* of the nucleus. The lifetime L of the metastable state is the simulation time from the start until the nucleation event; it must be much longer than the relaxation time: $L \gg \tau_{\rm rel} \approx (1-\Delta)^{-1}$ [7,31]. This condition determines the lifetime minimum in the numerical experiments. The lifetime maximum depends on the speed of the available computational facility: In the present work $L_{\max} = 8000$. Thus, there are three sources of systematic error in the estimate of the lifetime: the finite relaxation time, the nucleation criterion, and the cutoff simulation time. For the statistical analysis of the lifetime, we ran 100 trials of the simulations at the same conditions changing only values of the initial seed of the noise, averaged the lifetime and its moments over the trials, and calculated the mean value $\tau_L \equiv \langle L\rangle$ and variance $r_L \equiv \mathrm{var}(L)$. To find the probability density function of the lifetime $f(L)$ we constructed its probability mass histogram with 26 bins between the maximum and minimum values.

B. Results

In Fig. 3 are plotted typical time sequences of the fluctuating quantities $\mathcal{V}(t)$ and $\mathcal{H}(t)$ from the start until the nucleation event at two different sets of the control parameters. The equilibrium averages of these quantities are consistent with the perturbation-theory estimates, see Eq. (15) and Ref. [31]. Clearly, the volumetric content $\mathcal{V}(t)$ provides a more detailed representation of the path of the system in the configuration space $\{\eta\}$ than the Hamiltonian $\mathcal{H}(t)$. First, relaxation of $\mathcal{V}(t)$ to its equilibrium level takes longer than that of $\mathcal{H}(t)$ because the former is linearly proportional to the OP fluctuation modes, see Eq. (2), while the latter is composed of the contributions where the lowest order of the modes is quadratic, see Eqs. (1) and (7). Second, in large systems the cycling effect—visiting by the representative point of the system of the same set of states constituting a cycle before exiting the metastable domain [32]—is recognizable on the time sequence $\mathcal{V}(t)$ but not on $\mathcal{H}(t)$, see Fig. 3(a). In both cases depicted in Fig. 3 the lifetimes of the α phase are significantly larger than the relaxation times. Although one can easily identify on the time sequences $\mathcal{V}(t)$ and $\mathcal{H}(t)$, the nucleation moment—start of runaway from the vicinity of the α phase, e.g., Fig. 3(a)—the thermodynamic properties of the system at that moment, namely the free-energy barrier and the volumetric content of the critical nucleus, cannot be identified on these plots.

In Figs. 4–6 the 3D OP fields of the nucleated systems with the same parameters as in Fig. 3 are depicted in different projections. Clearly, the nucleation event results in formation of a compact nucleus with diffuse boundaries. The nucleus is supercritical because $\eta(\mathbf{x}_c) \geqslant 1$. Figures 4 are XY planes, which run through the centers of the nuclei. Differences in the nucleus sizes and fluctuation levels are clearly visible.

In Fig. 5 are plotted the OP field distributions along the Z axes, which run through the centers of the same nuclei as in Fig. 4. For comparison, in Fig. 5(a) is plotted the radial field distribution of the critical nucleus at the same supersaturation, cf. Fig. 1(b). It shows that the first stage of the supercritical evolution at large driving forces is the nucleus growth by the size and amplitude.

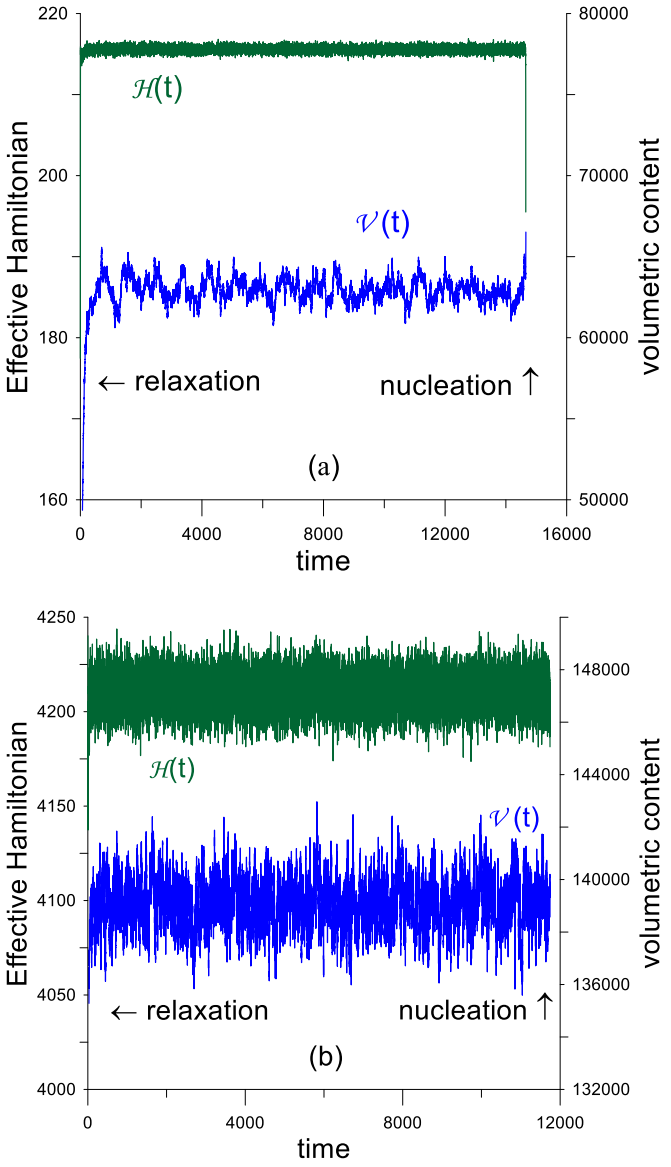

FIG. 3. Time sequences of $\mathcal{V}(t)$ and $\mathcal{H}(t)$ of the system with (a) $\Delta = 0.95$, $\varepsilon = 0.00087$, $V = 8 \times 10^6$ and (b) $\Delta = 0.7$, $\varepsilon = 0.029$, $V = 3.375 \times 10^6$. Arrows show the relaxation processes and the nucleation moments.

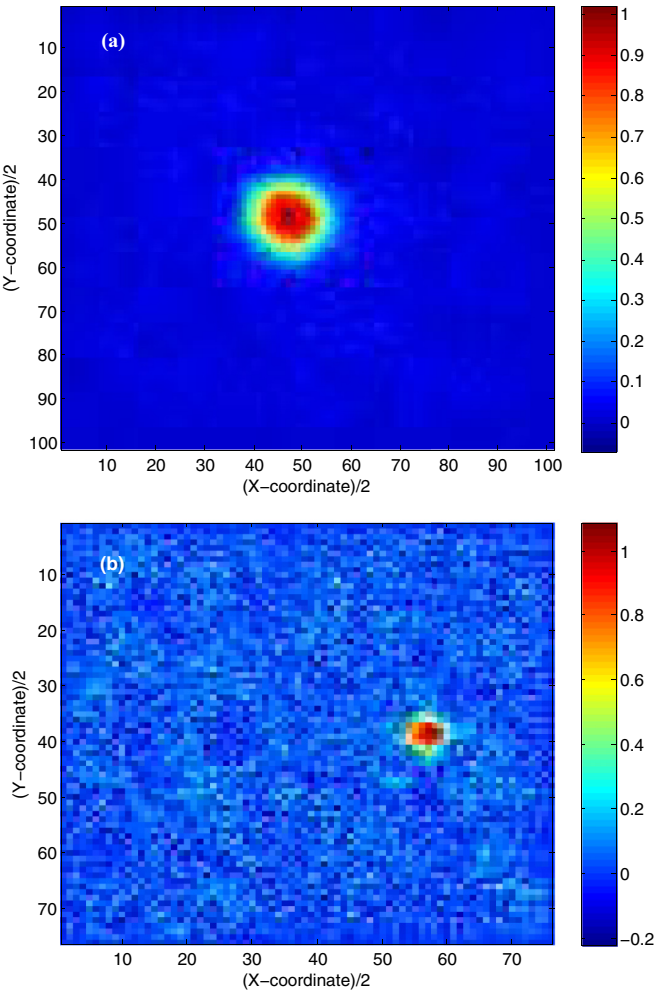

FIG. 4. OP distributions in XY planes through the centers of the nuclei: (a) $\Delta = 0.95$, $\varepsilon = 0.00087$, $V = 8 \times 10^6$ and (b) $\Delta = 0.7$, $\varepsilon = 0.029$, $V = 3.375 \times 10^6$.

In Fig. 6 is depicted the 2D orthographic projection of the level surface $\eta(\mathbf{x}) = 0.3333$ of the nucleus from Figs. 3(a), 4(a), and 5(a). It is almost nearly spherical. (Dependence of the sphericity of the nucleus on the control parameters was not analyzed in the present work.)

In Fig. 7 are plotted the numerically generated probability mass histograms of the lifetime at different values of the control parameters. Comparison of the histograms with the probability distribution functions of various distributions showed that the best fit was achieved by the lognormal distribution:

$$f(L) = \frac{1}{L\sqrt{2\pi \ln\left(1 + \frac{r_L}{\tau_L^2}\right)}} e^{-\frac{\ln^2 \frac{L\sqrt{\tau_L^2 + r_L}}{\tau_L^2}}{2\ln\left(1 + \frac{r_L}{\tau_L^2}\right)}}, \qquad (19)$$

where τ_L and r_L are, respectively, the mean value and variance of the lifetime L.

In Fig. 8 are plotted the logarithm of the mean lifetime τ_L as a function of the inverse noise intensity ε at different values of the supersaturation Δ. The plots are nearly straight lines with the slopes and y intercepts dependent on the supersaturation: The slopes decrease and the y intercepts increase with the increase of Δ.

In Fig. 9 are plotted the logarithm of the mean lifetime as a function of the logarithm of the volume of the system at different values of the supersaturation. The slope of the linear fit depends on the supersaturation: it approaches (-1) as $\Delta \to 0.5$ and $(-1/2)$ as $\Delta \to 1$.

C. Theoretical analysis

An important conclusion that can be made from the numerical experiments is that the thermodynamic properties of a fluctuating system, namely the free-energy excess and volumetric content of the nucleation barrier, cannot be directly measured from the fluctuation plots. In order to see that, one can compare thermodynamic formulae, Eq. (A21), with their

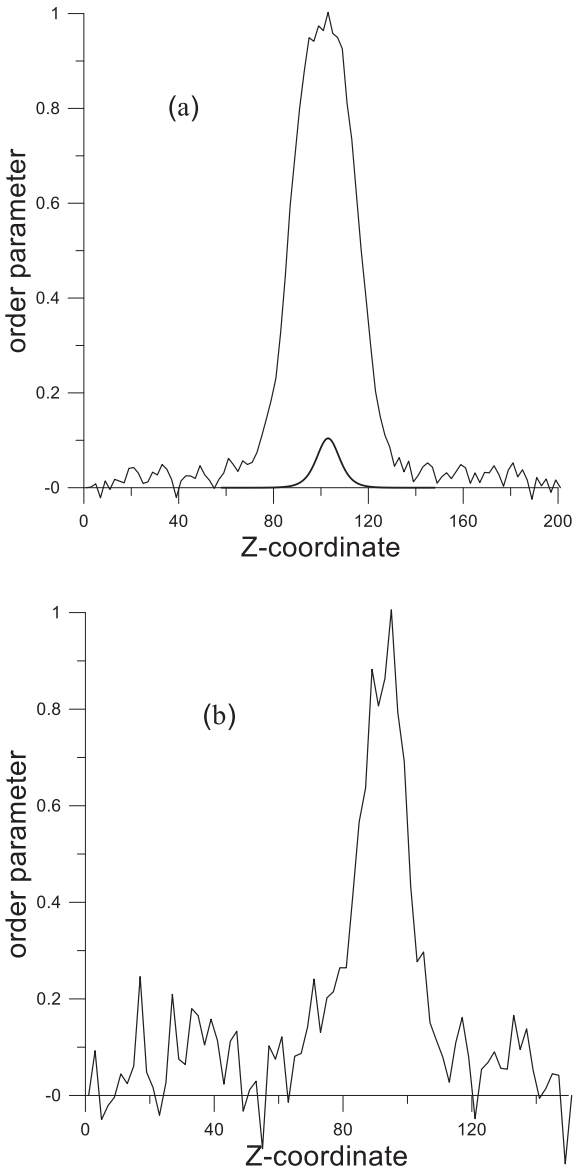

FIG. 5. OP distributions on the Z coordinates through the centers of the nuclei: (a) $\Delta = 0.95$, $\varepsilon = 0.00087$, $V = 8 \times 10^6$ and (b) $\Delta = 0.7$, $\varepsilon = 0.029$, $V = 3.375 \times 10^6$. Smooth curve in (a) represents the radial distributions of the critical nucleus with the same parameters, cf. Fig. 1(b).

fluctuation counterparts, Eq. (15), for a typical system of ($V = 8 \times 10^6$, $\Delta = 0.8$, and $\varepsilon = 0.01$) and notice that the thermodynamic quantities of the critical nucleus are even smaller than the dispersions of their fluctuation counterparts, let alone the quantities themselves. Hence, in order to find these quantities one has to develop indirect methods of observation.

Many of the numerical observations can be clarified if we cast the mean lifetime into the functional dependence suggested by the nucleation theories:

$$\tau_L = \frac{P(\Delta)}{V^{\alpha(\Delta)}} e^{\Delta F_B(\Delta)/\varepsilon}, \tag{20}$$

where the prefactor P and exponent α are functions of the supersaturation Δ. Taking the natural logarithm of this

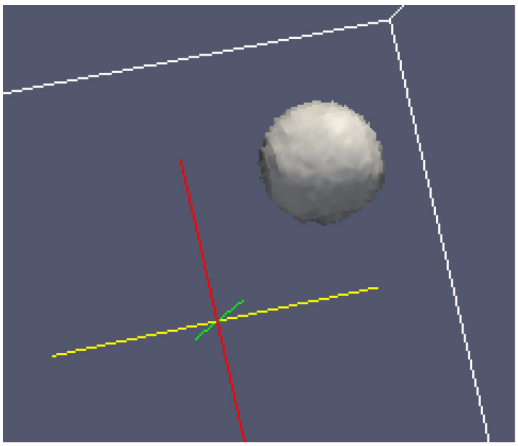

FIG. 6. 2D orthographic projection of the 3D nucleus at $\Delta = 0.95$, $\varepsilon = 0.00087$, $V = 8 \times 10^6$ (imaged by ParaView).

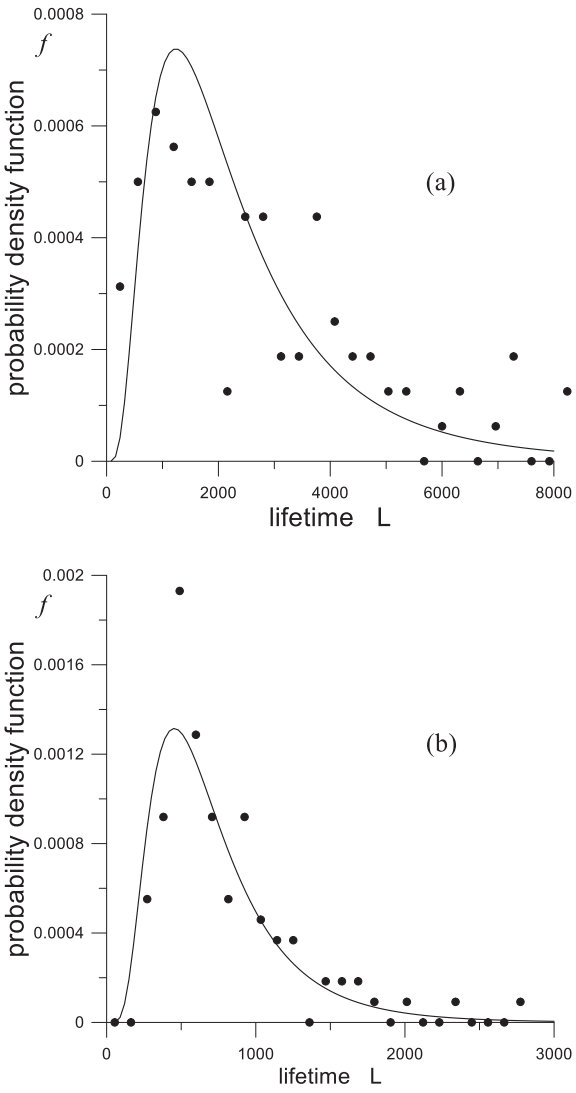

FIG. 7. Probability distribution histograms and lognormal probability distribution functions of lifetime in the systems of $V = 8 \times 10^6$ and (a) $\Delta = 0.7$, $\varepsilon = 0.029$ and (b) $\Delta = 0.9$, $\varepsilon = 0.00345$.

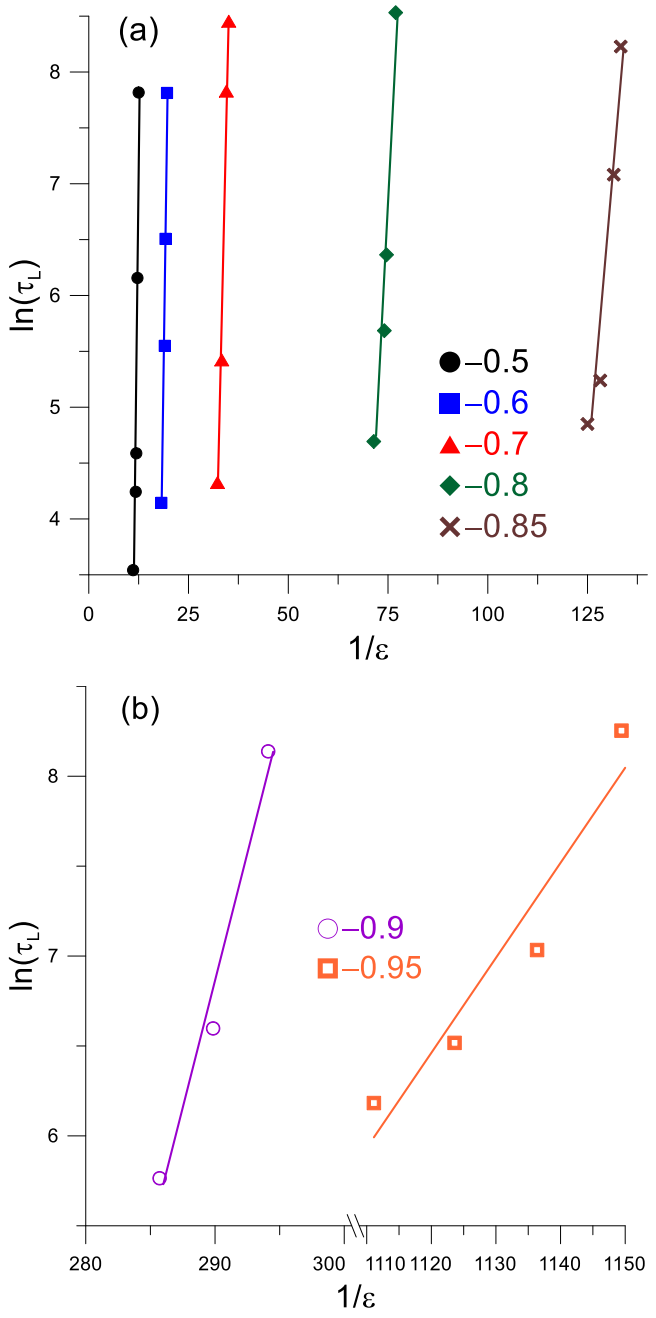

FIG. 8. Logarithm of the mean lifetime τ_L as a function of the inverse noise ε in the systems of $V = 8 \times 10^6$ at different values of the supersaturation Δ labeled by different symbols on (a) $\Delta = 0.5$–0.85 and (b) $\Delta = 0.9, 0.95$.

expression, we obtain:

$$\ln \tau_L = \ln P(\Delta) - \alpha(\Delta) \ln V + \Delta F_B(\Delta)\varepsilon^{-1}. \qquad (21)$$

Then the slope of $\ln(\tau_L)$ as a function of $(1/\varepsilon)$ for constant V and Δ should be equal to ΔF_B and the slope of $\ln(\tau_L)$ as a function of $\ln(V)$ for constant ε and Δ—to α. The slopes are tabulated in Table I and plotted in Fig. 10. Comparison of the former with the free-energy barrier ΔF_B from Eq. (A21) produced a good match. Then, application of the nucleation theorem, Eq. (11), yields the volumetric content of the critical

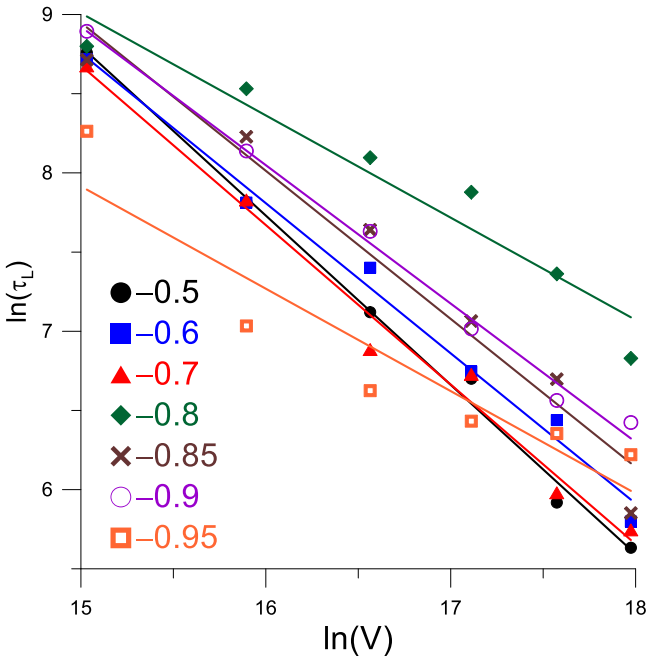

FIG. 9. Logarithm of the mean lifetime τ_L as a function of the logarithm of the volume V at different values of the supersaturation Δ labeled by different symbols.

nucleus, which should be compared to direct observations of the OP field in the numerical experiments, see Fig. 5. We also found (see Table I and Fig. 10) that the volume exponent α and prefactor P vary with the supersaturation Δ : $\alpha \approx 1$ as $\Delta \to 0.5$ while $\alpha \to 1/2$ as $\Delta \to 1$.

IV. DISCUSSION AND CONCLUSIONS

In this publication, using the Ginzburg-Landau approach, we developed a direct ("brute-force") numerical simulation method for observation of a 3D homogeneous nucleation process—creation of a critical nucleus out of fluctuations. Formation of a nucleus belongs to the category of rare events that have dramatic consequences for the system. The main observational quantity is the lifetime of a metastable state—not the nucleation rate—that is, time for the system to form a critical (to be exact, supercritical) nucleus. We start with a homogeneous metastable state subjected to the internal thermal noise and observe evolution of the system governed by the stochastic time-dependent Ginzburg-Landau equation. The lifetime was statistically averaged over 100 trials with different initial values of the seed for the random noise generator. The mean lifetime was analyzed as a function of the control parameters: supersaturation Δ, noise strength ε, and volume of the system V. In this publication, we used the asymmetric (no external field), athermal (temperature-independent driving force), tangential (simple phase diagram) Hamiltonian, which has two independent "drivers" of the phase transition: supersaturation and thermal noise. In the previous publication of the author [31], the method was verified by the fluctuation-perturbation theory for the metastable equilibrium states of the same Hamiltonian and the best parameters for the method were identified.

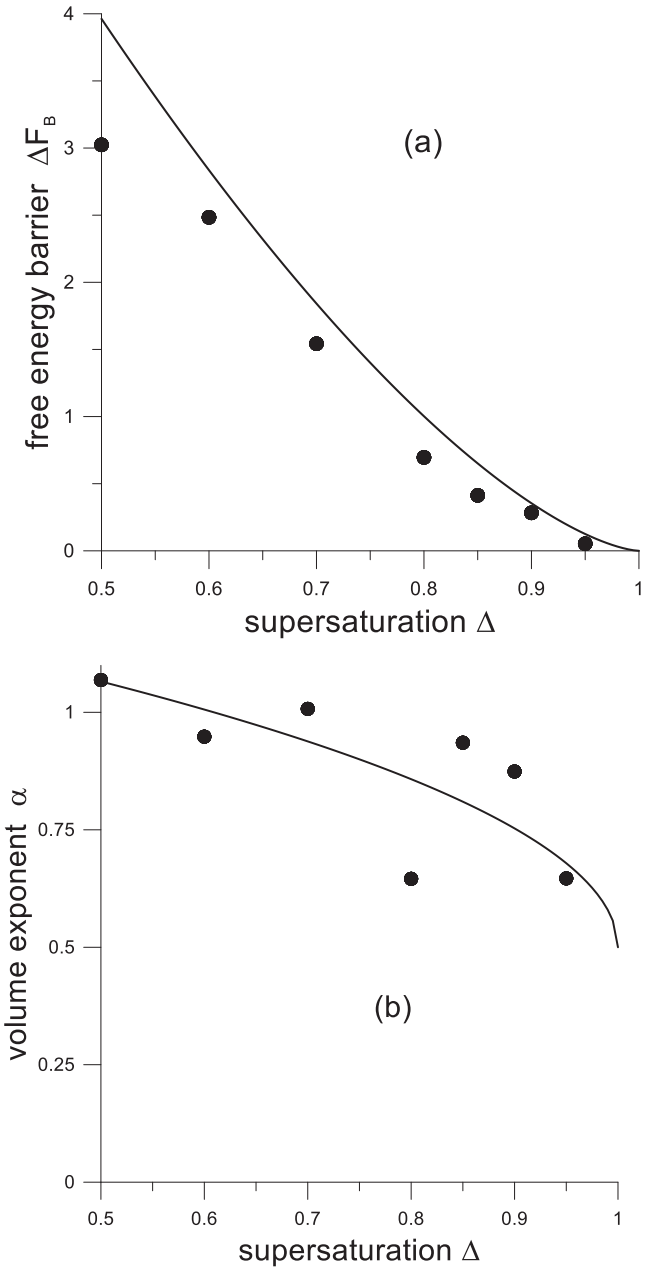

FIG. 10. Numerically generated slopes of $\ln(\tau_L)$ as a function of $(1/\varepsilon)$ for constant V (a) and as a function of ln(V) for constant ε (b) versus the supersaturation Δ. Solid lines: (a) ΔF_B from Eq. (A21); (b) a guide to eye.

Combination of the theory and numerical simulations helped us reveal many hidden features of the nucleation process. For instance, we found that the thermodynamic properties of the critical nucleus—its size and energy—cannot be found through the direct measurements of the "brute-force" method. The reason for that is that the fluctuation excess properties are proportional to the volume of the system while the respective thermodynamic ones are independent of that. Then, even for small (but not very small) systems, the former are significantly larger than the latter. In our observations, the thermodynamic excess properties happened to be even smaller than the dispersions of their respective fluctuation counterparts. It is impossible, so to speak, to unwrap the critical nucleus from the chaos of fluctuations. However, we found an indirect method to recover the free-energy barrier for nucleation ΔF_B from the fluctuation "experiments" (cf. Ref. [24]). It consists of measuring the mean lifetime and plotting its logarithm as a function of $(1/\varepsilon)$ at $V = \text{const}$ for different values of the supersaturation Δ. Then, according to Eq. (20), the slope of this plot is equal to the free-energy barrier. Inspection of the data in Table I shows that the ratio of the free-energy barrier to the strength of noise is very high: 30–70, hence, according to Eq. (20), the prefactor P is very small.

Moreover, we found that the dependence of the mean lifetime on the volume of the system itself depends on the supersaturation: The lifetime is inversely proportional to the volume for $\Delta \sim 0.5$ and inversely proportional to the square root of the volume for $\Delta \to 1$. This can be explained by stating that at large driving forces fluctuations in the neighboring volumes of the system are not independent. The functional dependence, Eq. (20), also explains the lognormal distribution of the lifetime. Indeed, we just need to recall that a quantity is distributed lognormally if it can be represented as an exponential function with a normally distributed exponent and that the thermal noise is a normally distributed stochastic quantity. Comparison of the numerically generated order parameter distribution of the supercritical nucleus with that of the theoretical critical one, Fig. 5(a), sheds light on the initial stage of the supercritical evolution of the system. It shows that the first stage of the supercritical evolution at the large driving force is growth of the nucleus by the size and amplitude.

The "brute-force" nucleation simulation method can be used only at large—more exactly, not small—supersaturations. This may be explained by the functional dependence, Eqs. (20) and (A14) and Fig. 2. Indeed, as the barrier becomes too high at $\Delta \to 0$ the lifetime becomes exponentially large. Hence, at small supersaturations one has to use other methods of

TABLE I. Comparison between numerical observations and theoretical calculations.

Supersaturation Δ	Noise strength ε	Free energy barrier ΔF_B	Volume exponent α	Prefactor P
0.5	0.08–0.09	3.0238	1.0688	2×10^{-6}
0.6	0.051–0.06	2.484	0.9482	5×10^{-12}
0.7	0.0285–0.031	1.5424	1.0074	1×10^{-13}
0.8	0.013–0.015	0.6957	0.7849	7×10^{-16}
0.85	0.0075–0.008	0.413	0.9354	1×10^{-14}
0.9	0.0034–0.004	0.2829	0.8741	2×10^{-27}
0.95	0.00087–0.0009	0.0528	0.6466	4×10^{-19}

TABLE II. Crystallization constants of metals.

Quantity **units**	T_m 10^{+3} K	σ J/m^2	R_0 10^{-10} m	$\tau=(\gamma W)^{-1}$ 10^{-14} s	$W=6\sigma/R_0$ 10^{+9} J/m^3	$\kappa=6\sigma R_0$ 10^{-10} J/m	γ 10^{+3} m^3/Js	$T_F=WR_0{}^3/k_B$ 10^{+3} K	$\varepsilon_m=T_m/T_F$
Aluminum	0.9335	0.115	2.5	6.08	2.76	1.73	5.96	3.12	0.299
Copper	1.3580	0.280	1.65	5.00	10.2	2.77	1.96	3.31	0.410
Nickel	1.7280	0.370	1.25	2.87	17.8	2.78	1.96	2.51	0.688

the nucleation simulation such as umbrella sampling [21], transition-path sampling [22], or multilevel splitting [17].

Experimentally, the large driving force of transformation can be achieved, for instance, by applying high pressure in isothermal crystallization of simple metals or other substances with large slopes of melting-temperature-pressure curves (dT_m/dP), e.g., alkali metals. Specifically, one needs to prepare the melt at temperature $T_m(0)$—melting point at $P=0$ (atmospheric pressure)—and apply hydrostatic pressure $P>0$. All liquids have spinodal pressures P_S at which they become absolutely unstable to crystallization. Then, the supersaturation is $\Delta\sim P/P_S$ and the noise strength is $\varepsilon_m=T_m/T_F$. Other parameters for typical metals (the author did not find the data on the alkali metals) are given in Table II. Inspection of the data shows that most of the metals are very "noisy" at their melting points.

Below we succinctly formulate the most important accomplishments and failures of the present research.

Accomplishments:

(1) We constructed a method capable of simulating the basic element of homogeneous nucleation.

(2) The method was "calibrated" by the perturbation theory.

(3) The method allowed us to study the homogeneous nucleation process and initial stages of the supercritical evolution.

(4) The method allowed us to study statistical properties of the lifetime and dependence of the lifetime on the control parameters: supersaturation, noise strength, and volume of the system.

(5) Although the thermodynamic properties of the nucleus cannot be obtained directly from the fluctuation properties of the system (the former is much smaller than the latter), we found an indirect method to extract these properties from the data on the lifetime.

(6) We also proved the nucleation theorem in the field approximation.

Failures:

(1) Calibration of the method was not perfect: The energy of the metastable phase did not follow its theoretical trend as a function of the supersaturation.

(2) The method cannot be used for small supersaturations.

ACKNOWLEDGMENTS

The author thanks Drs. J. Langer and V. Kalikmanov for helpful discussions. This work was performed under the financial assistance of the National Science Foundation's Award No. 1436120 from the U.S. Department of Commerce, National Institute of Standards and Technology, as part of the Center for Hierarchical Materials Design (CHiMaD).

APPENDIX A: THERMODYNAMIC PROPERTIES OF THE BARRIER STATE

To find the thermodynamic properties of the barrier state in the large isotropic system with free boundaries we need to solve the 3D spherically symmetric ELE, Eq. (4), with the Newmann-type BC, Eq. (5) for $\eta_B(r)$, where r is the radial distance from the center. In a system described by the tangential Hamiltonian, Eqs. (1) and (7), they take the form:

$$\kappa\left(\frac{d^2}{dr^2}+\frac{2}{r}\frac{d}{dr}\right)\eta_B+2W\eta_B(\eta_B-\eta_t)(1-\eta_B)=0, \quad \text{(A1)}$$

$$\eta_B\to 0, \quad \frac{d\eta_B}{dr}\to 0 \ \text{ for } \ r\to\infty. \quad \text{(A2)}$$

Equations (A1) and (A2) should be supplemented with the conditions at the center:

$$\frac{d\eta_B}{dr}=0 \ \text{ at } r=0. \quad \text{(A3)}$$

Then the volumetric content, Eq. (2), and free-energy excess, Eq. (6), of the barrier state can be expressed as follows:

$$v_B(\Delta)=4\pi\int_0^\infty \eta_B(r)\,r^2\,dr=4\pi\,I_1(\eta_B), \quad \text{(A4)}$$

$$\Delta F_B(\Delta)=4\pi\int_0^\infty\left\{H(\eta_B;\Delta)-\frac{1}{2}\eta_B\frac{\partial H}{\partial\eta}(\eta_B;\Delta)\right\}r^2dr$$
$$=\frac{4\pi}{3}W\left[(1+\eta_t)I_3(\eta_B)-\frac{3}{2}I_4(\eta_B)\right]. \quad \text{(A5)}$$

Here and below the moments are defined as:

$$I_n(f)\equiv\int_0^\infty f^n(r)\,r^2\,dr \quad \text{(A6)}$$

Equations (A1)—(A6) can be simplified using the scaling of Eq. (18):

$$\frac{r}{R_0}\to r; \quad \frac{I_n}{R_0^3}\to I_n; \quad \eta_B(r)\to\eta_B(r); \quad \frac{H(\eta)}{W}\to H(\eta). \quad \text{(A7)}$$

1. Small supersaturation limit

In order to find an analytical solution of Eq. (A1) for

$$\Delta\ll 1, \quad \text{(A8)}$$

we notice that, in this case, everywhere except for a small vicinity of the center, it is resolved by the kink-type 1D solution

of ELE, Eq. (9) [10,33]:

$$\eta_B(r) \cong \eta_I(r - R_N), \quad r > r_0 \sim o(1); \tag{A9}$$

where the constant, which may be called the *radius of the critical nucleus*, is

$$R_N = \frac{2}{\Delta}. \tag{A10}$$

To verify Eq. (A9), one needs to use the property $d\nu(\eta)/d\eta = 6\omega(\eta)$, see Eq. (7). In the vicinity of the center:

$$\eta_B(r) \cong \eta_B(0) + \frac{1}{6}\frac{\partial H}{\partial \eta}(\eta_B(0), \Delta) r^2, \quad 0 < r < r_0. \tag{A11}$$

Moreover, matching the solutions, Eq. (A9) and Eq. (A11), we obtain that

$$\eta_B(0) \cong \eta_I(-R_N) = 1 - \eta_I(R_N) \sim 1 - e^{-R_N}. \tag{A12}$$

Notice from Eqs. (A10) and (A12) that in the limit $\Delta \to 0$ the coefficient in front of r^2 in Eq. (A11) is exponentially small.

To calculate the free-energy barrier, Eq. (A5), we notice that the contribution of the domain $0 < r < r_0$, Eq. (A11), is negligible due to its small size. The domain $r_0 < r < \infty$ we divide into two subdomains: $r_0 < r < R_N - r_0$ and $R_N - r_0 < r < \infty$. Then the free-energy excess due to the barrier may be written as follows:

$$\Delta F_B = \frac{4\pi}{3}\left[(1+\eta_t)\eta_B^3(0) - \frac{3}{2}\eta_B^4(0)\right]\int_0^{R_N} r^2\, dr + 4\pi R_N^2 \int_{-\infty}^{+\infty}\left(\frac{d\eta_B}{dr}\right)^2 dr, \tag{A13}$$

where the integration limits in the first integral were changed because $R_N \gg r_0$ and in the second were spread to $\pm\infty$ due to Eqs. (A11) and (A12). Then, using properties of the 1D kink-type solution, Eq. (10), we obtain the relationships for the free-energy excess:

$$\Delta F_B = 4\pi R_N^2 \frac{1}{6} - \frac{4\pi}{3} R_N^3 \frac{\Delta}{6} = \frac{2\pi R_N^2}{9} = \frac{8\pi}{9\Delta^2} \tag{A14}$$

and volumetric content of the barrier state:

$$v_B = \frac{4\pi}{3} R_N^3 = \frac{32\pi}{3\Delta^3}. \tag{A15}$$

They agree with the respective expressions of CNT in the scaled form. The unbounded growth of the free-energy barrier in the limit of the vanishing driving force ($\Delta \to 0$) is due to its growing size, Eq. (A10), and flatness, Eqs. (A9), (A11), and (A12).

2. Large supersaturation limit

The large supersaturation (the so-called scaling or Cahn-Hilliard [34]) limit of nucleation takes place when the system approaches the α-spinodal point, that is:

$$\Delta \to 1^-. \tag{A16}$$

In this case, the OP of the transition state

$$\eta_t \to 0^+ \tag{A17}$$

provides the relevant scale for the OP spatial distributions, see Eq. (A1). For instance, the scaled correlation radius diverges:

$$R_C = \frac{1}{\sqrt{2\eta_t}} = \frac{1}{\sqrt{1-\Delta}} \to \infty. \tag{A18}$$

The variables in Eqs. (A1)–(6) can be rescaled further as follows:

$$r = \frac{\rho}{\sqrt{\eta_t}};\ \eta_B(r) = \eta_t\, Y(\rho);\ \ I_n(\eta_B) = \eta_t^{n-3/2} \mathrm{I}_n(Y). \tag{A19}$$

Noticing that in this regime $\eta_t < \eta_B \ll 1$ we obtain from Eq. (A1) the following parameterless equation for the scaled barrier state $Y(\rho)$:

$$\left(\frac{d^2}{d\rho^2} + \frac{2}{\rho}\frac{d}{d\rho}\right) Y + 2Y(Y-1) = 0, \tag{A20}$$

with the boundary conditions that follow from Eqs. (A2) and (A3). Asymptotically, $Y \sim e^{-\rho/R_C}/\rho$ where $R_C = 2^{-1/2}$. Relations for the scaled moments of the barrier state are known: $\mathrm{I}_1(Y) = \mathrm{I}_2(Y) = {}^1\!/_2 \mathrm{I}_3(Y)$ (see Ref. [35] or Appendix B). Then, using Eqs. (A4) and (A5), we obtain expressions for the free-energy excess:

$$\Delta F_B = \frac{2\pi\sqrt{2}\,\mathrm{I}_1(Y)}{3}(1-\Delta)^{3/2} \to 0 \tag{A21}$$

and volumetric content of the barrier state:

$$v_B = \frac{4\pi \mathrm{I}_1(Y)}{(1-\Delta)^{1/2}} \to \infty. \tag{A22}$$

3. Intermediate supersaturations

To find the thermodynamic properties of the barrier state for the medium values of the supersaturation, ELE, Eq. (A1) with the BC, Eqs. (A2) and (A3) were scaled as in Eq. (A7) and solved numerically using the shooting method. Specifically, for given Δ, first, the value of $\eta_B(0)$ was set equal to $(1+\eta_c)/2$ where $H(\eta_c, \Delta) = 0$ and $0 < \eta_c < 1$. Second, $\eta_B(r_0)$ was calculated using Eq. (A12) for $r_0 = 0.005$. Third, using this value as the initial condition, Eq. (A1) was integrated in the domain $r_0 < r \leqslant r_f$, where $r_f > \max(R_N, R_C)$, using Runge-Kutta method with adaptive step-size control. Fourth, $\eta_B(r_f)$ was verified against the boundary conditions, Eq. (A2), the value of $\eta_B(0)$ was adjusted accordingly, and the calculations were repeated from step (2); the iterations of $\eta_B(0)$ were repeated 24 times. Fifth, the integration domain boundary r_f was increased by 10% and, provided the change was not significant, the trajectory $\eta_B(r)$ was recorded. Using the previously recorded trajectory of $\eta_B(r)$ the moments, Eq. (A6) were calculated. Same procedure was used to solve the scaled Eq. (A20) in the large-supersaturation regime; the latter yielded $Y(0) = 4.192$, $Y(R_C) = 2.585$, and $\mathrm{I}_1(Y) = 3.784$, which is in accord with Ref. [35]. In Figs. 1 and 2, the black curves represent numerically calculated distributions $\eta_B(\mathrm{r})$ and functions $\Delta F_B(\Delta)$, $v_B(\Delta)$.

APPENDIX B: INTEGRAL RELATIONS

First, we present the ELE, Eq. (A20), and BC, Eqs. (A2) and (A3), in the form [35]:

$$\frac{1}{\rho}\frac{d^2}{d\rho^2}(\rho Y) + 2Y(Y-1) = 0 \tag{B1}$$

$$\frac{dY}{d\rho}(0) = 0, \quad \frac{dY}{d\rho}(\infty) \to 0, \quad Y(\infty) \to 0. \tag{B2}$$

Then, multiplying Eq. (B1) by ρ^2, integrating from 0 to ∞ using the rules of integration by parts and BC, Eq. (B2), and using Eq. (A6), we obtain the relation:

$$\mathrm{I}_2(Y) = \mathrm{I}_1(Y). \tag{B3}$$

Next, multiplying Eq. (B1) by $\rho^2 Y$ and following the same procedure as before, we obtain the relation:

$$\int_0^\infty \left(\frac{dY}{d\rho}\right)^2 \rho^2\, d\rho \equiv J(Y) = 2[\mathrm{I}_3(Y) - \mathrm{I}_2(Y)]. \tag{B4}$$

Furthermore, multiplying Eq. (B1) by $\rho^3 dY/d\rho$ and following the same procedure as before, we obtain:

$$J(Y) = 2[2\mathrm{I}_3(Y) - 3\mathrm{I}_2(Y)]. \tag{B5}$$

Finally, simultaneous solution of Eqs. (B4) and (B5) yields:

$$J(Y) = \mathrm{I}_3(Y), \tag{B6}$$

$$\mathrm{I}_3(Y) = 2\mathrm{I}_2(Y). \tag{B7}$$

APPENDIX C: NUCLEATION THEOREM

To prove the nucleation theorem we differentiate Eq. (6) with respect to μ and obtain:

$$\frac{\partial \Delta F_E}{\partial \mu} = \int_V d^3x \left[\frac{\partial H}{\partial \mu} + \frac{1}{2}\left(\frac{\partial \eta_E}{\partial \mu}\frac{\partial H}{\partial \eta} - \eta_E \frac{\partial \eta_E}{\partial \mu}\frac{\partial^2 H}{\partial \eta^2} - \eta_E \frac{\partial^2 H}{\partial \eta \partial \mu}\right)\right]. \tag{C1}$$

For a kink-type state described by Eqs. (9) and (A9), all terms in the parenthesis of the integrand vanish everywhere except the narrow transition region of thickness $2R_0$. For the first term of the integrand, we find from Eq. (7) that

$$\frac{\partial H}{\partial \mu} \approx \eta. \tag{C2}$$

Comparing Eqs. (C1) and (C2) with Eq. (2) we find the nucleation theorem, Eq. (11). Eqs. (C1) and (C2) show that the nucleation theorem is due to the general properties of the Hamiltonian, Eq. (1), not due to the specific form of Eq. (7).

[1] J. W. Christian, *The Theory of Phase Transformations in Metals and Alloys* (Pergamon, Oxford, 1965), p. 418.
[2] R. W. Balluffi, S. M. Allen, and W. C. Carter, *Kinetics of Materials* (Wiley, Hoboken, NJ, 2005), p. 459.
[3] V. I. Kalikmanov, *Nucleation Theory* (Springer, New York, 2013).
[4] D. W. Oxtoby and R. Evans, J. Chem. Phys. **89**, 7521 (1988).
[5] L. Granasy, J. Non-Cryst. Solids **219**, 49 (1997).
[6] L. D. Landau and E. M Lifshitz, *Statistical Physics* (Pergamon Press, Oxford, 1958).
[7] A. Umantsev, *Field Theoretic Method in Phase Transformations* (Springer, New York, 2012).
[8] J. S. Langer, Ann. Phys. **41**, 108 (1967); **54**, 258 (1969); J. D. Gunton and M. Droz, *Introductions to the Theory of Metastable and Unstable States* (Springer-Verlag, Berlin, 1983), p. 84.
[9] M. Buttiker and R. Landauer, Phys. Rev. A **23**, 1397 (1981).
[10] W. Klein, Phys. Rev. Lett. **47**, 1569 (1981); D. W. Herrmann, W. Klein, and D. Stauffer, *ibid.* **49**, 1262 (1982); C. Unger and W. Klein, Phys. Rev. B **29**, 2698 (1984); **31**, 6127 (1985).
[11] K. Binder, Phys. Rev. B **8**, 3423 (1973).
[12] A. Z. Patashinskii and B. I. Shumilo, Zh. Eksp. Teor. Fiz. **77**, 1417 (1979) [Sov. Phys. JETP **50**, 712 (1979)].
[13] A. Umantsev and G. B. Olson, Phys. Rev. E **48**, 4229 (1993).
[14] R. S. Maier and D. L. Stein, Phys. Rev. Lett. **87**, 270601 (2001); E. Vanden-Eijnden and M. G. Westdickenberg, J. Stat. Phys. **131**, 1023 (2008).
[15] O. Penrose and J. L. Lebowitz, J. Stat. Phys. **3**, 211 (1971).
[16] F. Cerou, A. Guyader, T. Lelievre, and F. Malrieu, ALEA, Lat. Am. J. Probab. Math. Stat. **10**, 359 (2013).
[17] J. Rolland, F. Bouchet, and E. Simonnet, J. Stat. Phys. **162**, 277 (2016).
[18] H. Tomita and S. Miyashita, Phys. Rev. B **46**, 8886 (1992).
[19] M. J. Mandell, J. P. McTague, and A. Rahman, J. Chem. Phys. **64**, 3699 (1976); C. S. Hsu and A. Rahman, *ibid.* **71**, 4974 (1979).
[20] K. Yasuoka and M. Matsumoto, J. Chem. Phys. **109**, 8451 (1998); **109**, 8463 (1998).
[21] P. R. ten Wolde, M. J. Ruiz-Montero, and D. Frenkel, Phys. Rev. Lett. **75**, 2714 (1995); S. Auer and D. Frenkel, Nature **413**, 711 (2001).
[22] P. G. Bolhuis, D. Chandler, C. Dellago, and P. L. Geissler, Annu. Rev. Phys. Chem. **53**, 291 (2002); C. Dellago, P. G. Bolhuis, F. S. Csajka, and D. Chandler, J. Chem. Phys. **108**, 1964 (1998).
[23] S. Auer and D. Frenkel, Annu. Rev. Phys. Chem. **55**, 333 (2004).
[24] J. Wedekind, R. Strey, and D. Reguera, J. Chem. Phys. **126**, 134103 (2007); J. Wedekind and D. Reguera, J. Phys. Chem. B **112**, 11060 (2008).
[25] L. Granasy, T. Borzsonyi, and T. Pusztai, Phys. Rev. Lett. **88**, 206105 (2002); T. W. Heo, L. Zhang, Q. Du, and L-Q. Chen, Script. Mater. **63**, 8 (2010).
[26] R. Petschek and H. Metiu, J. Chem. Phys. **79**, 3443 (1983).
[27] O.T. Valls and G.F. Mazenko, Phys. Rev. B **34**, 7941 (1986).
[28] P. Meakin, H. Metiu, R. Petschek, and D.J. Scalapino, J. Chem. Phys. **79**, 1948 (1983).
[29] $y = \mathrm{const}(x)$ means that quantity y is independent of x but may depend on other quantities.
[30] D. Kashchiev, J. Chem. Phys. **76**, 5098 (1982); **118**, 1837 (2003); V. I. Kalikmanov, *ibid.* **129**, 044510 (2008).

[31] D. Uzinov and A. Umantsev, Physica A **448**, 283 (2016).
[32] E. N. M. Cirillo, F. R. Nardi, and J. Sohier, J. Stat. Phys. **161**, 365 (2015).
[33] P. V. Gordon, S. A. Kukushkin, and A. V. Osipov, Phys. Solid State **44**, 2175 (2002).
[34] J.W. Cahn and J. E. Hilliard, J. Chem. Phys. **28**, 258 (1958).
[35] G. Wilemski and J.-S. Li, J. Chem. Phys. **121**, 7821 (2004).